Optics & Laser Technology 181 (2025) 111887

Contents lists available at ScienceDirect

Optics and Laser Technology

journal homepage: www.elsevier.com/locate/optlastec

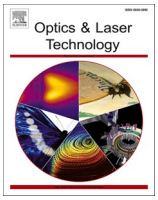

Full length article

High efficiency broadband parametric amplification assisted by second harmonic generation

Zhihao Wang [a], Lu Xu [a,*], Shuangxi Peng [a], Feilong Hu [a], Dong Zhao [b], Zuofei Hong [c], Qingbin Zhang [a,d,*], Peixiang Lu [a,c,d]

[a] Wuhan National Laboratory for Optoelectronics and School of Physics, Huazhong University of Science and Technology, Wuhan 430074, China
[b] School of Electronic and Information Engineering, Hubei University of Science and Technology, Xianning 437100, China
[c] Hubei Key Laboratory of Optical Information and Pattern Recognition, Wuhan Institute of Technology, Wuhan 430025, China
[d] Optics Valley Laboratory, Hubei 430074, China

ARTICLE INFO

Keywords:
Ultrafast laser
Optical parametric amplification
Back conversion suppression

ABSTRACT

In typical scenarios, quadratic nonlinear processes such as second harmonic generation (SHG) and sum frequency generation (SFG) that accompany optical parametric amplification (OPA) are often considered unfavorable parasitic effects. These effects can lead to a reduction in energy conversion efficiency during OPA. In this study, we demonstrate an approach to enhance OPA efficiency by eliminating the signal pulse through SHG in a simple collinear geometry while maintaining a broadband output using a femtosecond pump laser. The complete setup features a three-stage OPA system, with the final stage employing a hybrid OPA-SHG process that effectively suppresses back conversion, achieving up to 60.8 % pump depletion and 26.2 % pump-to-idler energy conversion, resulting in an idler energy of 0.97 mJ. By harnessing the capabilities of a broadband femtosecond pump and Type-I phase matching to enhance phase-matched bandwidth, we generated a 1.85-μm idler pulse with a near-transform-limited (TL) duration of 33.5 fs through compression in a silicon window. Furthermore, we maintained excellent beam quality and output power stability, with only 0.23 % root mean square (RMS) fluctuations over the course of one hour. This mid-IR laser source, operating at the millijoule (mJ) level and characterized by its high beam quality, is exceptionally well-suited for advancing attosecond and strong-field research.

1. Introduction

Over the past decades, intense femtosecond lasers have significantly advanced strong-field science, attosecond science, and nonlinear optics [1–3]. The lasers based on chirped pulse amplification (CPA) typically have a fixed wavelength due to the limited bandwidth of the gain medium, which restricts their tuning range. Optical parametric amplification (OPA) offers several advantages over chirped pulse amplification (CPA), including lower thermal load, broad gain bandwidth, and flexible wavelength tunability [4,5]. Consequently, significant efforts have been made to develop mid-infrared (MIR) tunable pulses using OPA [6,7]. These pulses provide advantages over fixed near-infrared (NIR) pulses in applications such as time-resolved optical spectroscopy [8], high-harmonic generation [9], and the creation of isolated attosecond pulses [10].

However, back conversion [11] in the parametric process limits conversion efficiency, with pump depletion typically not exceeding 50 % [12–16]. This inefficiency is mainly due to non-uniform pump extraction, especially with Gaussian temporal profiles. To address this, time and space pulse shaping has been proposed [17,18]. Spatiotemporal flat-top laser pulses can effectively increase pump depletion. However, the complexity of pump shaping techniques poses challenges for nanosecond pulses and is even less applicable to femtosecond pulses. Additionally, at high pump depletion, idler pulses hinder further energy transfer from the pump to signal pulses, causing back conversion [19,20]. Several schemes have been proposed to improve OPA conversion efficiency by dissipating idler pulses. Quasi-parametric amplification (QPA) is a representative scheme. By doping the nonlinear crystal with ions that absorb idler pulses during amplification process, the back conversion is suppressed [21,22]. Recently, QPA based on cascaded nonlinear frequency conversion has been proposed [23,24]. In addition, there are other schemes such as quasi-phase matching (QPM)

* Corresponding authors.
E-mail addresses: luxu_0909@hust.edu.cn (L. Xu), zhangqingbin@hust.edu.cn (Q. Zhang).

https://doi.org/10.1016/j.optlastec.2024.111887
Received 13 July 2024; Received in revised form 29 August 2024; Accepted 27 September 2024
Available online 10 October 2024

configuration walk-off [25], high reflection coating [26], and non-collinear pump recycling schemes [27,28]. However, compared to typical OPA solutions, these approaches often require exotic materials or consume significant space. Furthermore, to achieve high energy conversion, these schemes typically use picosecond or nanosecond pump pulses, so that the effect of temporal walk-off, which also affects pump depletion, is negligible. Moreover, due to the low pump intensity, thicker nonlinear crystals are required to achieve saturation in the amplification process, severely limiting the gain bandwidth. Consequently, even after compression, the durations of the amplified pulses exceed several hundred femtoseconds. In contrast, the ultrashort femtosecond pump has the advantage of containing more wavelength components than the picosecond or nanosecond pump, supporting broadband phase matching and amplification for few-cycle pulses [29,30]. Moreover, the femtosecond pump can achieve high peak intensity more easily, requiring only thinner crystals for saturation amplification and thus minimizing gain narrowing.

In this paper, we propose a hybrid OPA-SHG scheme to suppress back conversion in femtosecond OPA. The final power amplifier uses a single nonlinear crystal in a collinear geometry, eliminating the need for complex laser or medium fabrication designs. Unlike previous methods that improved pump depletion by removing idler pulses, our approach improves efficiency by eliminating signal pulses instead. In this system, the signal pulse generated in the crystal is simultaneously converted to its second harmonic (SH), thereby eliminating back conversion. This allows the idler pulse to be efficiently amplified to higher energy while maintaining good beam quality. The broadband idler pulse supports a sub-five-cycle TL duration, which can also serve as an idea input for the post-compression stage, leading to even shorter few-cycle and potentially single-cycle regions [31–33].

2. Phase matching in BBO crystal

The premise of generating efficient broadband idler pulses by eliminating signal pulses is that broadband phase matching bandwidth of OPA and signal SHG processes can be simultaneously achieved in the nonlinear crystal. This bandwidth is determined by the phase-matching efficiency $sinc^2(\Delta kL/2)$, where Δk is the wave vector mismatch and L is the crystal thickness. The wave vector mismatches for OPA and SHG are given by $\Delta k_{OPA} = k_p - k_s - k_i$ and $\Delta k_{SHG} = k_{2s} - 2k_s$, respectively. Here, k_j ($j = p, s, i$ and $2s$) represents the wave vector of the pump, signal, idler, and signal SH pulses, respectively. BBO is a negative uniaxial birefringent crystal with a large gain bandwidth for Type-I OPA pumped at 0.8 μm. It also has a high nonlinear coefficient ($d_{eff} \approx 2pm/V$) and a high damage threshold ($200GW/cm^2$). These properties ensure that efficient energy conversion can be achieved in a thinner crystal, minimizing the adverse effects of temporal walk-off.

The collinear phase-matching conditions for Type-I OPA and SHG in the BBO crystal are illustrated in Fig. 1. The pump wavelength of OPA is fixed at 0.8 μm. Fig. 1(a) shows the phase matching curves. A magic point appears at a crystal orientation of $\theta = 20.13°$, where simultaneous phase matching occurs for a 1.4 μm signal, corresponding to a 0.7 μm signal SH and a 1.85 μm idler. For Type-II OPA at this wavelength, the phase matching angle is $\theta = 26.09°$, which is significantly far from SHG. At this magic phase matching angle, the wave vector mismatch Δk for OPA and SHG are illustrated in Fig. 1(b). As mentioned above, the phase matching bandwidth is determined by $sinc^2(\Delta kL/2)$. Therefore, $|\Delta kL| < \pi$ is necessary to generate effective amplification. In BBO-based ultrashort femtosecond pumped OPA experiments, the crystal thickness in the power amplification stage typically ranges from 2 to 4 mm. Therefore, $|\Delta k| < 1mm^{-1}$ is used as a criterion for phase matching bandwidth here. As shown in Fig. 1(b), for $|\Delta k| < 1mm^{-1}$, the bandwidths of the OPA and SHG are 228 nm and 60 nm, respectively, which are sufficient to support the hybrid OPA-SHG process pumped by a broadband femtosecond laser. It is expected to generate broadband idler pulses with spectrum ranges spanning from 1700 nm to 2000 nm. Additionally, the wave vector mismatch for idler SHG is marked with a red circle, showing a large vector mismatch ($\Delta k > 7.5mm^{-1}$) that prevents idler dissipation.

3. Experimental setup

The experimental setup is illustrated in Fig. 2. The pump source in the setup is a commercially available Ti: sapphire laser operating at 800 nm, delivering 30 fs, 5 mJ at a 1 kHz repetition rate. The pump pulse is split into two beams by a beam splitter. One beam (1.3 mJ) pumps a two-stage OPA system [29,35]. In this setup, the beam is divided into three parts. The smallest part (~10 μJ) is focused onto a 3 mm-thick sapphire plate after passing through a variable attenuator for white light continuum (WLC) generation, which serves as the seed source. A fraction of the pump pulses (~90 μJ) is used to pump the first OPA stage. A small noncollinear angle (<1°) is used for separating the output pulses. The WLC is amplified to ~ 3 μJ in the first BBO crystal (BBO-1) with a center wavelength of 1.4 μm. The pump and idler pulses are blocked by a beam dump. The amplified 1.4 μm signal pulse is further amplified in the second BBO crystal (BBO-2) using a 1.2 mJ pump pulse. The pump and idler pulses are separated using two dichroic mirrors. At the output of the two-stage OPA, a 150 μJ, 1.4 μm signal pulse is obtained to serve as the seed pulse for the hybrid OPA-SHG stage. The BBO crystals used in the two-stage OPA are cut for Type-II phase matching (θ = 27.2°, φ = 30°) with thicknesses of 2.5 mm and 2 mm. Type-II crystals are used instead of Type-I to generate a higher energy and narrower bandwidth 1.4 μm pulse, which is more beneficial for efficient amplification in the subsequent hybrid OPA-SHG stage.

The other part of the laser energy (3.7 mJ) is used as the pump for the

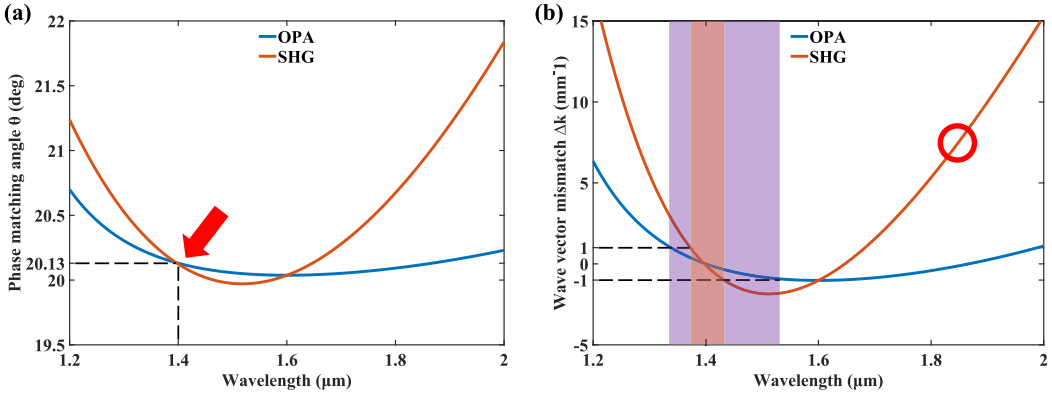

Fig. 1. (a) Phase matching curves and (b) Wavevector mismatch curves for Type-I OPA (blue lines) and SHG (orange lines). The pump wavelength for OPA is fixed at 0.8 μm and the crystal orientation used in (b) is given by θ = 20.13°. (Sellmeier coefficients taken from [34].).

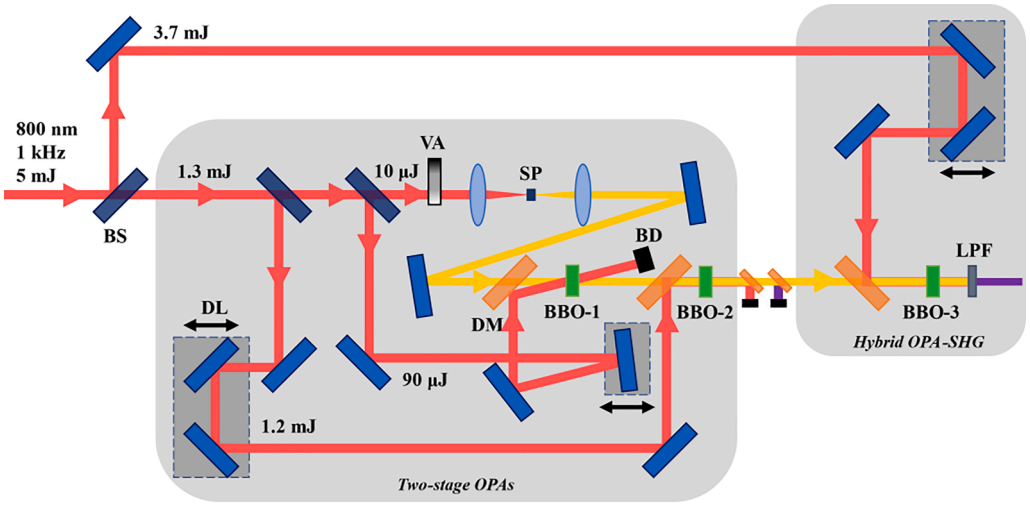

Fig. 2. Schematic setup of the system. BS, beam splitter; VA, variable attenuator; SP, sapphire plate; DL, delay line; DM, dichroic filter; BD, beam dump; LPF, long-pass filter. The pre-amplification consists of a two-stage OPA process, and the power-amplification is a hybrid OPA-SHG process.

hybrid OPA-SHG stage. In this power amplification stage, a Type-I phase matching BBO crystal, cut at $\theta = 20^\circ$ and $\varphi = 0^\circ$, is used for high-efficiency idler amplification. The pump pulses and the signal pulses in the three stages are combined using dichroic mirrors. Temporal overlap in these stages is achieved using the delay lines. After sufficient amplification, the pump and signal pulses are separated by a long-pass filter, and the idler pulse is compressed using a silicon window.

In OPA pumped by ultrashort femtosecond pulses, temporal walk-off, caused by the relative group delay accumulated during propagation, significantly affects pump depletion. When the relative group delay exceeds the pulse lengths, the pulses do not temporally overlap anymore and their interaction vanishes. The pulse-splitting length evaluates the effect of temporal walk-off: $L_{jk} = |\frac{\tau}{\delta_{jk}}| = |\tau/(\frac{1}{v_{gj}} - \frac{1}{v_{gk}})|$. Here, τ represents the full width at half-maximum (FWHM) of the pump pulses, δ_{jk} represents the group velocity mismatch (GVM) between the interacting pulses, v_{gj} *and* v_{gk} $(j,k = p,s,i \text{ and } 2s)$ represent the group velocities of the pump, signal, idler, and signal SH pulses, respectively. For fixed crystal type and pulse wavelengths, the group velocity mismatch is also fixed. The pulse-splitting length becomes longer with increasing pulse duration. The group velocity mismatch between the interacting pulses is illustrated in Fig. 3, based on Type-I BBO crystal and 800 nm pump wavelength. At the 1.4 μm signal wavelength, the group velocity mismatches are: $\delta_{s-p} = 9.5 fs/mm$, $\delta_{i-p} = 22.4 fs/mm$ and $\delta_{2s-s} = 17.8 fs/mm$. Therefore, to avoid the effects of temporal walk-off and achieve effective amplification within a suitable crystal thickness (~2–4 mm), the pump pulse duration is slightly chirped to ~60 fs. This is achieved by optimizing the grating-based compressor in the Ti: sapphire laser system without further dispersion management.

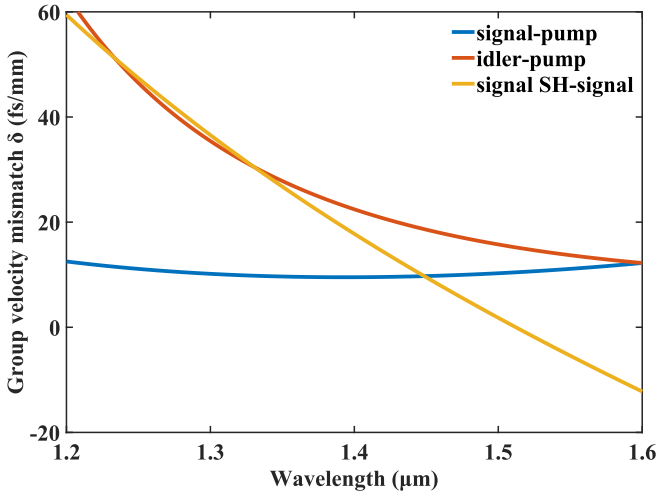

Fig. 3. Group velocity mismatch between the interacting pulses as a function of the wavelength for Type-I OPA and SHG. The pump wavelength for OPA is fixed at 0.8 μm.

4. Experimental results and discussion

In the hybrid OPA-SHG stage, different thicknesses of Type-I phase-matching BBO crystals are used to evaluate the effect of the simultaneous OPA and SHG. Fig. 4 (a) shows the signal and idler conversion efficiency as a function of the BBO thickness at the pump energy of 3.7 mJ. The energy at 0 mm thickness represents the incident pulse of the seed signal with an energy of 150 μJ. By fine-tuning the BBO angle and the pump-to-signal delay, a maximum idler energy of 0.97 mJ is achieved with a crystal thickness of 3 mm, corresponding to 26.2 % pump-to-idler energy conversion efficiency and 60.8 % pump energy depletion. The signal pulse energy remains low at all thicknesses, except for a slight increase when amplified by a 1 mm thick crystal. In this hybrid OPA-SHG process, the Manley-Rowe relation is still satisfied between the idler and pump. However, due to the strong SHG process, the signal no longer obeys this relation. The numerical simulation results based on the four-wave coupling equation[23,36] are also presented in Fig. 4 (a). Although there are some discrepancies between the measured results and the calculations, the measured conversion efficiency exhibits a similar trend to the calculated results. For comparison, we also perform experiments using a typical OPA process based on Type-II phase-matching BBO at the same wavelength. For common femtosecond OPAs, the two types of phase-matching are characterized as follows: Type-I has a larger gain bandwidth, while Type-II offers higher energy conversion [5]. As shown in Fig. 4 (a), using Type-II phase-matching BBO, a high pump-to-idler energy conversion efficiency of 17 % and a pump depletion close to 40 % are obtained. In contrast, the maximum pump energy depletion of the hybrid OPA-SHG scheme is increased by more than 50 %. Additionally, Fig. 4 (b) presents the spectra of the amplified idler pulses for both types of phase-matching with 3 mm thick crystals. The FWHM bandwidth of Type-I is 103 nm, which is wider than the 82 nm of Type-II. This indicates that, compared to typical OPA, the hybrid OPA-SHG scheme simultaneously achieves high pump depletion and broad bandwidth.

To further demonstrate the role of OPA and SHG in the amplification process, we measured the signal and idler pulse spectra for different BBO

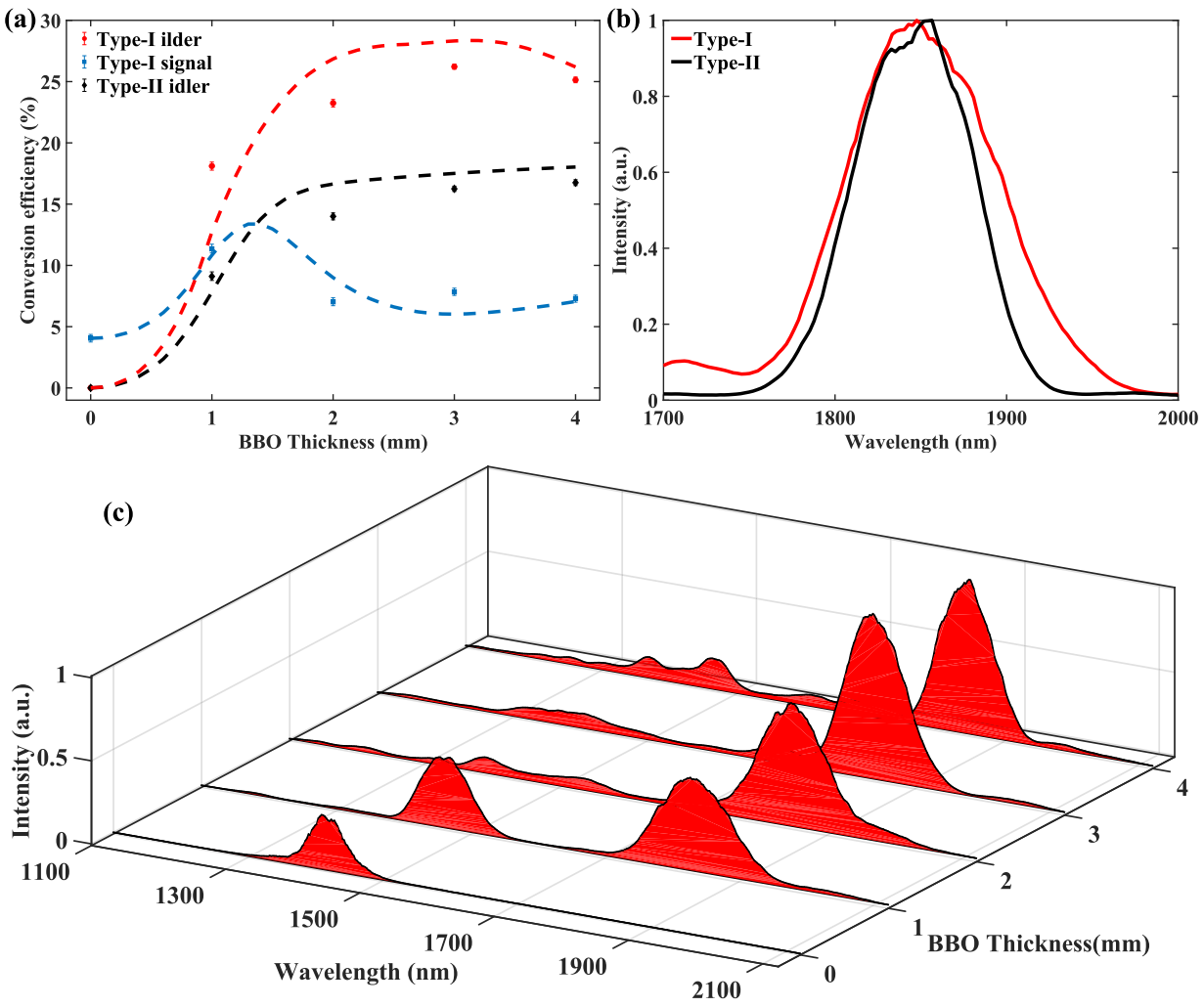

Fig. 4. (a) Measured conversion efficiency versus crystal thickness for Type-I idler (red circles), Type-I signal (blue squares), and Type-II idler (black diamonds). The dashed lines are simulation results, respectively. (b) Amplified idler spectra for Type-I (red) and Type-II (black). (c) Amplified spectra versus crystal thickness for Type-I hybrid OPA-SHG.

thicknesses in the hybrid OPA-SHG scheme. As shown in Fig. 4 (c), the spectra intensities are normalized to their energies. The spectrum at 0 mm thickness represents the incident seed signal pulse. The idler spectra maintain Gaussian-like intensity profiles across all thicknesses. In contrast, the signal spectra behave differently from the idler pulses. Initially, the pump pulse intensity is much stronger than the signal pulse. For the signal pulse, the gain from OPA is much greater than the loss from SHG. The signal pulse exhibits a Gaussian-like profile when amplified with a 1 mm thick crystal. As thicker crystals are used, the pump pulse intensity gradually decreases during amplification. For the signal pulse, the gain from OPA and the loss from SHG reach a dynamic equilibrium, meaning almost all the energy from the pump pulse flows into the signal SH pulse. Consequently, the signal pulse intensity remains low, allowing pump energy to keep flowing into the idler, ultimately achieving high pump depletion. Due to the strong SHG, the signal pulse spectra exhibit modulation. Notably, back conversion still occurs with a 4 mm thick crystal. This is mainly due to the narrower phase-matching bandwidth of the SHG. While OPA can generate a broadband signal pulse, the spectral components outside the center wavelength of the signal pulse cannot be dissipated in time by SHG, resulting in a dip at the center wavelength of the signal spectrum.

The pulse duration is measured using a home-built second-harmonic-generation frequency-resolved optical gating (SHG-FROG). The uncompressed idler pulse has a duration of 59.2 fs with a negative GDD of approximately 390 fs^2. Therefore, a 0.4 mm silicon window is used for compression, and its effective thickness is varied by rotating the plate to achieve optimal compression. The results of the compressed pulse are shown in Fig. 5, with a 256 × 256 grid size and a reconstruction error of 0.003. The spectrum spans 1600–2100 nm with a FWHM bandwidth of 103 nm, supporting a sub-five-cycle TL pulse duration of 28.7 fs. The spectrum is accurately retrieved from SHG-FROG, and the idler pulse is compressed to 33.5 fs, close to the TL duration. For comparison, the compressed pulse duration of Type-II OPA is 42.6 fs. Consequently, the peak intensity of the idler pulse is nearly doubled using the hybrid OPA-SHG scheme. Finally, the energy stability of the idler pulse is recorded and plotted in Fig. 6 (a). Due to saturated amplification, the system demonstrates high robustness, achieving an RMS fluctuation of only 0.23 % over one hour, close to that of the pump laser (~0.21 %). Additionally, the far-field spot is measured by focusing the output beam with an f = 400 mm lens, as shown in Fig. 6 (b). The beam spot exhibits an excellent circular profile with a Gaussian cross-section in both the horizontal and vertical directions.

According to the above analysis, the phase-matching bandwidth of the signal pulse also affects the energy conversion in the hybrid OPA-SHG process. Further improvements in pump depletion and energy scaling can be achieved by combining the proposed scheme with dual-chirped OPA (DC-OPA) [36,37]. By applying the same chirp values to the pump and idler pulses, a narrow-bandwidth signal pulse can be

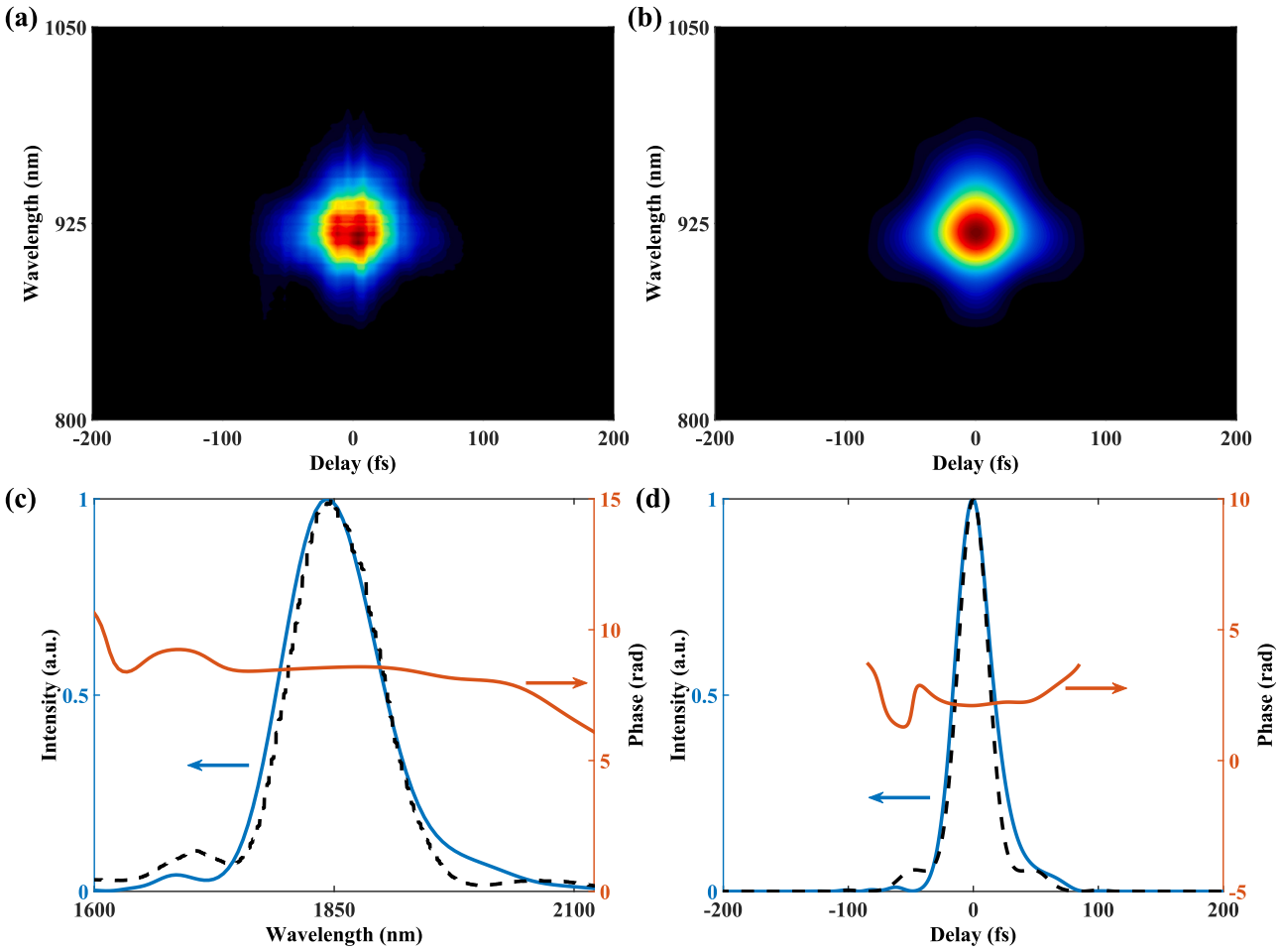

Fig. 5. (a) Measured FROG trace. (b) retrieved FROG trace. (c) retrieved spectrum (blue), measured spectrum (black), and phase (orange) of the compressed idler pulse. (d) temporal envelope (blue), phase (red), and TL pulse (black dashed line).

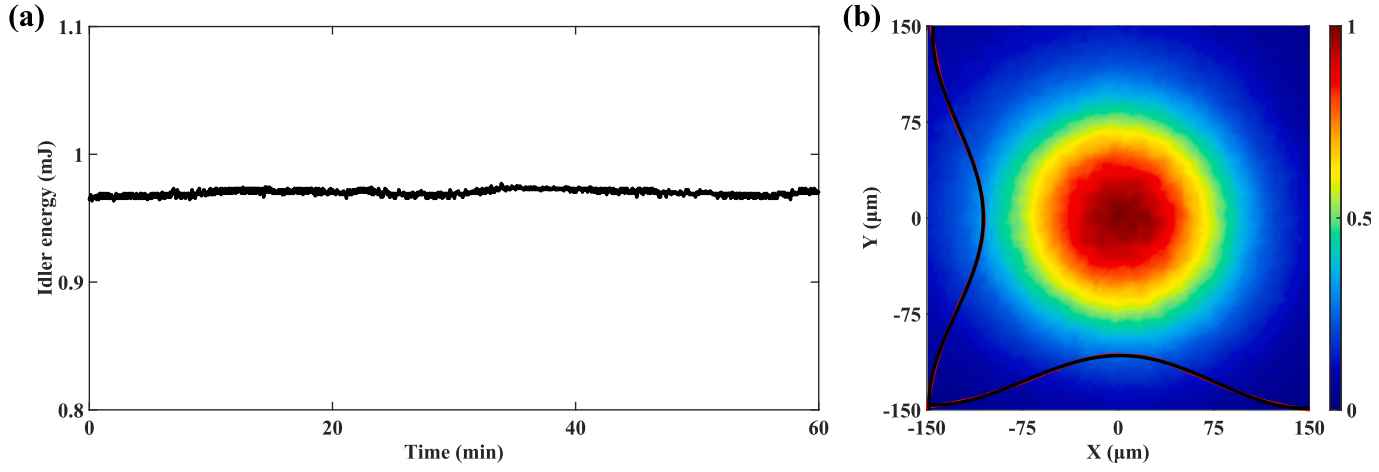

Fig. 6. (a) Energy stability of the idler pulse. (b) Spatial profile of focused idler beam, and the cross sections (red) and the gaussian fitting (black) of the beam.

generated while still producing a broad-bandwidth, few-cycle idler pulse. Additionally, pulse broadening reduces the adverse effects of temporal walk-off and increases the energy scalability of the hybrid OPA-SHG. In our experiments, high-efficiency idler pulse amplification is achieved when the signal pulse wavelength is 1.4 μm, corresponding to an idler wavelength of 1.85 μm. By introducing a non-collinear angle between the pump and seed pulses, a tunable range of idler wavelengths can be achieved, even for high-efficiency amplification of signal pulses, as shown in Fig. 7 (a). Since signal SHG only occurs at one angle for a given wavelength set, the signal tuning curves (yellow lines) can be determined first. Based on this, there are two sets of solutions for each pair of pump and signal wavelengths, as shown by blue and red lines in Fig. 7 (with solid and dashed lines distinguishing between the two solutions). A wide wavelength tuning range exists with non-collinear

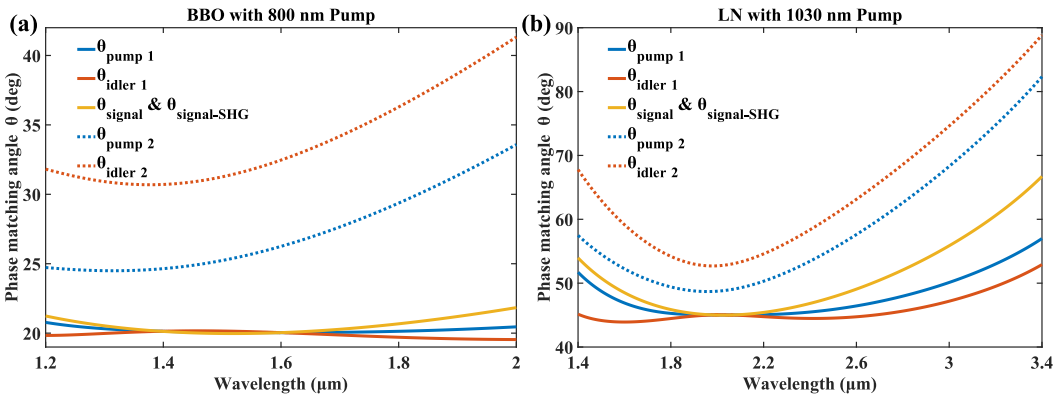

Fig. 7. Phase-matching angles for hybrid OPA-SHG. (a) BBO crystal pumped at 800 nm. (b) $LiNbO_3$ (LN) crystal pumped at 1030 nm. Two non-collinear configurations are possible across the signal tuning range, indicated by solid lines ($\theta_{pump\ 1}$, $\theta_{idler\ 1}$) and dashed lines ($\theta_{pump\ 2}$, $\theta_{idler\ 2}$), which share a common θ_{signal} that is fixed at the signal SHG phase-matching angle. (Sellmeier coefficients taken from [34,38]).

angles. Compared to the dashed-curve solutions, the solid-curve solutions in Fig. 7 have smaller noncollinear angles between the interacting pulses, making them more suitable for practical application. In Fig. 7 (a), aside from the degeneracy solution at 1.6 um, the only collinear solution is at 1.4 um, used in our experiments. Furthermore, the hybrid OPA-SHG scheme is not limited to the 0.8 μm Ti: sapphire laser. For example, 1.03 μm Yb-based femtosecond fiber lasers, which have narrower bandwidths and longer pulse durations, can be combined with LN or CSP crystals to achieve high efficiency mid-IR OPA tuning from 2-3.5 μm, as shown in Fig. 7 (b).

5. Conclusion

In summary, we have demonstrated a hybrid OPA-SHG scheme for generating broad bandwidth IR pulses with high conversion efficiency. By simultaneously satisfying the OPA and SHG phase-matching conditions in a Type-I BBO crystal and using a femtosecond pump, back-conversion circumvention, and broad bandwidth are achieved. The mJ-level, 33.5 fs, 1.85 μm idler pulse is achieved with a total pump depletion of 60.8 % and pump-to-idler efficiency of 26.2 %. The output laser exhibited good beam quality and energy stability. Additionally, the presented scheme can be applied to various types of lasers and used with different nonlinear crystals. We believe that the hybrid OPA-SHG will be a promising approach for efficiently increasing IR pulse energy and advancing strong-field physics research.

Funding

This work was supported by the National Natural Science Foundation of China (NSFC) (Grant Nos.92150106, 12174133, 12021004, and 11934006), the Innovation Project of Optics Valley Laboratory (No. OVL2021ZD001), the Major Program (JD) of Hubei Province (No.203BAA015) and the Cross Research Support Program of Huazhong University of Science and Technology (No.2023JCYJ041).

CRediT authorship contribution statement

Zhihao Wang: Writing – original draft, Visualization, Validation, Software, Methodology, Investigation, Formal analysis, Data curation. **Lu Xu:** Writing – review & editing. **Shuangxi Peng:** Validation, Investigation, Formal analysis, Data curation. **Feilong Hu:** Methodology, Investigation. **Dong Zhao:** Resources. **Zuofei Hong:** Methodology, Investigation. **Qingbin Zhang:** Writing – review & editing, Validation, Supervision, Resources, Project administration, Funding acquisition, Conceptualization. **Peixiang Lu:** Project administration, Funding acquisition.

Declaration of competing interest

The authors declare that they have no known competing financial interests or personal relationships that could have appeared to influence the work reported in this paper.

Data availability

Data underlying the results presented in this Letter are not publicly available at this time but may be obtained from the authors upon reasonable request.

References

[1] T. Brabec, F. Krausz, Intense few-cycle laser fields: Frontiers of nonlinear optics, Rev. Mod. Phys. 72 (2000) 545–591, https://doi.org/10.1103/RevModPhys.72.545.
[2] E. Goulielmakis, M. Schultze, M. Hofstetter, V.S. Yakovlev, J. Gagnon, M. Uiberacker, A.L. Aquila, E.M. Gullikson, D.T. Attwood, R. Kienberger, F. Krausz, U. Kleineberg, Single-cycle nonlinear optics, Science 320 (2008) 1614–1617, https://doi.org/10.1126/science.1157846.
[3] D. Kinyua, H. Long, X. Xing, S. Njoroge, K. Wang, B. Wang, P. Lu, Gigahertz acoustic vibrations of Ga-doped ZnO nanoparticle array, Nanotechnology 30 (2019), https://doi.org/10.1088/1361-6528/ab1739.
[4] G. Cerullo, S. De Silvestri, Ultrafast optical parametric amplifiers, Rev. Sci. Instrum. 74 (2003) 1–18, https://doi.org/10.1063/1.1523642.
[5] C. Manzoni, G. Cerullo, Design criteria for ultrafast optical parametric amplifiers, J. Opt. 18 (2016) 103501, https://doi.org/10.1088/2040-8978/18/10/103501.
[6] D. Sanchez, M. Hemmer, M. Baudisch, S.L. Cousin, K. Zawilski, P. Schunemann, O. Chalus, C. Simon-Boisson, J. Biegert, 7 μm, ultrafast, sub-millijoule-level mid-infrared optical parametric chirped pulse amplifier pumped at 2 μm, Optica 3 (2016) 147. https://doi.org/10.1364/OPTICA.3.000147.
[7] S. Cheng, Compact Ho:YLF-pumped ZnGeP 2 -based optical parametric amplifiers tunable in the molecular fingerprint regime, Opt. Lett. 45 (2020) 2255, https://doi.org/10.1364/OL.389535.
[8] D. Göries, B. Dicke, P. Roedig, N. Stübe, J. Meyer, A. Galler, W. Gawelda, A. Britz, P. Geßler, H. Sotoudi Namin, A. Beckmann, M. Schlie, M. Warmer, M. Naumova, C. Bressler, M. Rübhausen, E. Weckert, A. Meents, Time-resolved pump and probe x-ray absorption fine structure spectroscopy at beamline P11 at PETRA III, Rev. Sci. Instrum. 87 (2016) 053116, https://doi.org/10.1063/1.4948596.
[9] T. Popmintchev, M.-C. Chen, D. Popmintchev, P. Arpin, S. Brown, S. Ališauskas, G. Andriukaitis, T. Balčiunas, O.D. Mücke, A. Pugzlys, A. Baltuška, B. Shim, S. E. Schrauth, A. Gaeta, C. Hernández-García, L. Plaja, A. Becker, A. Jaron-Becker, M. M. Murnane, H.C. Kapteyn, Bright coherent ultrahigh harmonics in the keV X-ray regime from mid-infrared femtosecond lasers, Science 336 (2012) 1287–1291, https://doi.org/10.1126/science.1218497.
[10] F. Silva, S.M. Teichmann, S.L. Cousin, M. Hemmer, J. Biegert, Spatiotemporal isolation of attosecond soft X-ray pulses in the water window, Nat. Commun. 6 (2015) 6611, https://doi.org/10.1038/ncomms7611.
[11] G.W. Baxter, J.G. Haub, B.J. Orr, Backconversion in a pulsed optical parametric oscillator: evidence from injection-seeded sidebands, J. Opt. Soc. Am. B 14 (1997) 2723–2730, https://doi.org/10.1364/JOSAB.14.002723.
[12] E.J. Takahashi, T. Kanai, Y. Nabekawa, K. Midorikawa, 10 mJ class femtosecond optical parametric amplifier for generating soft x-ray harmonics, Appl. Phys. Lett. 93 (2008) 041111, https://doi.org/10.1063/1.2960352.

[13] C. Zhang, P. Wei, Y. Huang, Y. Leng, Y. Zheng, Z. Zeng, R. Li, Z. Xu, Tunable phase-stabilized infrared optical parametric amplifier for high-order harmonic generation, Opt. Lett. 34 (2009) 2730, https://doi.org/10.1364/OL.34.002730.
[14] N. Thiré, S. Beaulieu, V. Cardin, A. Laramée, V. Wanie, B.E. Schmidt, F. Légaré, 10 mJ 5-cycle pulses at 1.8 μm through optical parametric amplification, Appl. Phys. Lett. 106 (2015), https://doi.org/10.1063/1.4914344, 091110.
[15] B.E. Schmidt, P. Béjot, M. Giguère, A.D. Shiner, C. Trallero-Herrero, É. Bisson, J. Kasparian, J.-P. Wolf, D.M. Villeneuve, J.-C. Kieffer, P.B. Corkum, F. Légaré, Compression of 1.8 μm laser pulses to sub two optical cycles with bulk material, Appl. Phys. Lett. 96 (2010) 121109, https://doi.org/10.1063/1.3359458.
[16] S.L. Cousin, F. Silva, S. Teichmann, M. Hemmer, B. Buades, J. Biegert, High-flux table-top soft x-ray source driven by sub-2-cycle, CEP stable, 1.85-μm 1-kHz pulses for carbon K-edge spectroscopy, Opt. Lett. 39 (2014) 5383, https://doi.org/10.1364/OL.39.005383.
[17] V. Bagnoud, I.A. Begishev, M.J. Guardalben, J. Puth, J.D. Zuegel, 5 Hz, >250 mJ optical parametric chirped-pulse amplifier at 1053 nm, Opt. Lett. 30 (2005) 1843–1845, https://doi.org/10.1364/OL.30.001843.
[18] J.A. Fülöp, Zs. Major, B. Horváth, F. Tavella, A. Baltuška, F. Krausz, Shaping of picosecond pulses for pumping optical parametric amplification, Appl. Phys. B 87 (2007) 79–84, https://doi.org/10.1007/s00340-006-2488-3.
[19] D.D. Lowenthal, CW periodically poled LiNbO/sub 3/ optical parametric oscillator model with strong idler absorption, IEEE J. Quantum Electron. 34 (1998) 1356–1366, https://doi.org/10.1109/3.704319.
[20] G. Rustad, G. Arisholm, Ø. Farsund, Effect of idler absorption in pulsed optical parametric oscillators, Opt. Express 19 (2011) 2815, https://doi.org/10.1364/OE.19.002815.
[21] J. Ma, J. Wang, P. Yuan, G. Xie, K. Xiong, Y. Tu, X. Tu, E. Shi, Y. Zheng, L. Qian, Quasi-parametric amplification of chirped pulses based on a Smˆ3+-doped yttrium calcium oxyborate crystal, Optica 2 (2015) 1006, https://doi.org/10.1364/OPTICA.2.001006.
[22] J. Ma, K. Xiong, P. Yuan, X. Tu, J. Wang, G. Xie, Y. Zheng, L. Qian, Demonstration of 85% pump depletion and 10–6 noise content in quasi-parametric chirped-pulse amplification, Light Sci Appl 11 (2022) 269, https://doi.org/10.1038/s41377-022-00967-6.
[23] N. Flemens, N. Swenson, J. Moses, Efficient parametric amplification via simultaneous second harmonic generation, Opt. Express 29 (2021) 30590, https://doi.org/10.1364/OE.437864.
[24] Q. Lin, J. Ma, Z. Yin, P. Yuan, J. Wang, G. Xie, L. Qian, Optical modification of nonlinear crystals for quasi-parametric chirped-pulse amplification, Fundamental Research 4 (2024) 43–50, https://doi.org/10.1016/j.fmre.2022.05.021.
[25] Y. Li, H. Zhong, J. Yang, S. Wang, D. Fan, Versatile backconversion-inhibited broadband optical parametric amplification based on an idler-separated QPM configuration, Opt. Lett. 42 (2017) 2806, https://doi.org/10.1364/OL.42.002806.
[26] H. Cao, S. Tóth, M. Kalashnikov, V. Chvykov, K. Osvay, Highly efficient, cascaded extraction optical parametric amplifier, Opt. Express 26 (2018) 7516, https://doi.org/10.1364/OE.26.007516.
[27] X. Liang, X. Xie, J. Kang, Q. Yang, H. Wei, M. Sun, J. Zhu, Design and experimental demonstration of a high conversion efficiency OPCPA pre-amplifier for petawatt laser facility, High Pow Laser Sci Eng 6 (2018) e58, https://doi.org/10.1017/hpl.2018.52.
[28] X. Liang, X. Xie, C. Zhang, J. Kang, Q. Yang, P. Zhu, A. Guo, H. Zhu, S. Yang, Z. Cui, M. Sun, J. Zhu, Broadband main OPCPA amplifier at 808 nm wavelength in high deuterated DKDP crystals, Opt. Lett. 43 (2018) 5713, https://doi.org/10.1364/OL.43.005713.
[29] S.A. Rezvani, Z. Hong, X. Pang, S. Wu, Q. Zhang, P. Lu, Ultrabroadband tunable OPA design using a spectrally broadened pump source, Opt. Lett. 42 (2017) 3367, https://doi.org/10.1364/OL.42.003367.
[30] A.S. Wyatt, P. Matía-Hernando, A.S. Johnson, D.T. Matselyukh, A.J.H. Jones, R.T. Chapman, C. Cacho, D.R. Austin, J.W.G. Tisch, J.P. Marangos, E. Springate, Optical Parametric Amplification of Mid-Infrared Few-Cycle Pulses, (2019). http://arxiv.org/abs/1909.05954 (accessed October 1, 2023).
[31] M. Seo, K. Tsendsuren, S. Mitra, M. Kling, D. Kim, High-contrast, intense single-cycle pulses from an all thin-solid-plate setup, Opt. Lett. 45 (2020) 367–370, https://doi.org/10.1364/OL.382592.
[32] F. Hu, Z. Wang, Q. Yao, W. Cao, Q. Zhang, P. Lu, Clean hundred-μJ-level sub-6-fs blue pulses generated with helium-assisted solid thin plates, Opt. Lett. 48 (2023) 2555–2558, https://doi.org/10.1364/OL.487415.
[33] M. Müller, J. Buldt, H. Stark, C. Grebing, J. Limpert, Multipass cell for high-power few-cycle compression, Opt. Lett. 46 (2021) 2678–2681, https://doi.org/10.1364/OL.425872.
[34] G. Tamošauskas, G. Beresnevičius, D. Gadonas, A. Dubietis, Transmittance and phase matching of BBO crystal in the 3–5 μm range and its application for the characterization of mid-infrared laser pulses, Opt. Mater. Express 8 (2018) 1410, https://doi.org/10.1364/OME.8.001410.
[35] Z. Hong, F. Hu, X. Fu, W. Cao, Q. Zhang, P. Lu, Few-cycle 19-μm pulse generation via collinear spectrum synthesis in multiple-crystal OPA, Opt. Lett. 44 (2019) 3438, https://doi.org/10.1364/OL.44.003438.
[36] Q. Zhang, E.J. Takahashi, O.D. Mücke, P. Lu, K. Midorikawa, Dual-chirped optical parametric amplification for generating few hundred mJ infrared pulses, Opt. Express 19 (2011) 7190, https://doi.org/10.1364/OE.19.007190.
[37] Z. Hong, Q. Zhang, S.A. Rezvani, P. Lan, P. Lu, Tunable few-cycle pulses from a dual-chirped optical parametric amplifier pumped by broadband laser, Opt. Laser Technol. 98 (2018) 169–177, https://doi.org/10.1016/j.optlastec.2017.07.042.
[38] D.E. Zelmon, D.L. Small, D. Jundt, Infrared corrected Sellmeier coefficients for congruently grown lithium niobate and 5 mol% magnesium oxide –doped lithium niobate, J. Opt. Soc. Am. B 14 (1997) 3319, https://doi.org/10.1364/JOSAB.14.003319.